Molecularly imprinted nanoparticles reveal new insights into Pyk2 tyrosine kinase regulatory features

Tania M. Palhano Zanela[1], Milad Zangiabadi[2], Yan Zhao[2], Eric S. Underbakke[1]***.**

[1]Roy J. Carver Department of Biochemistry, Biophysics, and Molecular Biology, Iowa State University, Ames, IA, 50011, United States; Correspondence: esu@iastate.edu

[2]Department of Chemistry, Iowa State University, Ames, Iowa 50011, United States

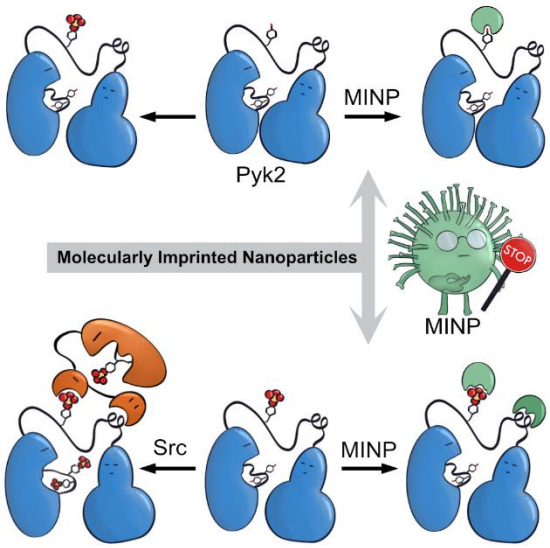

Abstract

Pyk2 is a multi-domain non-receptor tyrosine kinase that serves dual roles as signaling enzyme and scaffold. Pyk2 activation involves a multi-stage cascade of conformational rearrangements and protein interactions initiated by autophosphorylation of a linker site. Linker phosphorylation recruits Src kinase, and Src-mediated phosphorylation of the Pyk2 activation loop confers full activation. The regulated accessibility of the initial Pyk2 autophosphorylation site remains unclear. We employed peptide-binding molecularly imprinted nanoparticles (MINPs) to probe the regulatory conformations controlling Pyk2 activation. MINPs differentiating local structure and phosphorylation state revealed that the Pyk2 autophosphorylation site is protected in the autoinhibited state. Activity profiling of Pyk2 variants implicated FERM and linker residues responsible for constraining the autophosphorylation site. MINPs targeting each Src docking site disrupt the higher-order kinase interactions critical for activation complex maturation. Ultimately, MINPs targeting key regulatory motifs establish a useful toolkit for probing successive activational stages in the higher-order Pyk2 activation complex.

Introduction

Proline-rich tyrosine kinase 2 (Pyk2) is a non-receptor tyrosine kinase expressed in the brain and hematopoietic cells[1–3]. Pyk2 signaling tunes multiple physiological processes, including cell proliferation, neuronal development, and synaptic plasticity[4,5]. Dysregulation of Pyk2 activity has been implicated in various pathological conditions including cancer[6–8], cardiovascular diseases[9], and neurological disorders[10,11]. Pyk2 shares a domain organization and significant sequence similarity (65%) with its paralog focal adhesion kinase (FAK), including an N-terminal FERM regulatory domain, a central kinase domain, and a C-terminal focal adhesion targeting (FAT) domain (Figure 1A). Despite architectural similarities to FAK, Pyk2 has undergone evolutionary divergence, developing unique activation inputs and regulatory mechanisms. Whereas FAK is canonically activated by integrin receptor clustering at focal adhesions[12], the cytoplasmic Pyk2 has adopted Ca^{2+} sensitivity in neuronal cells[1,13–16].

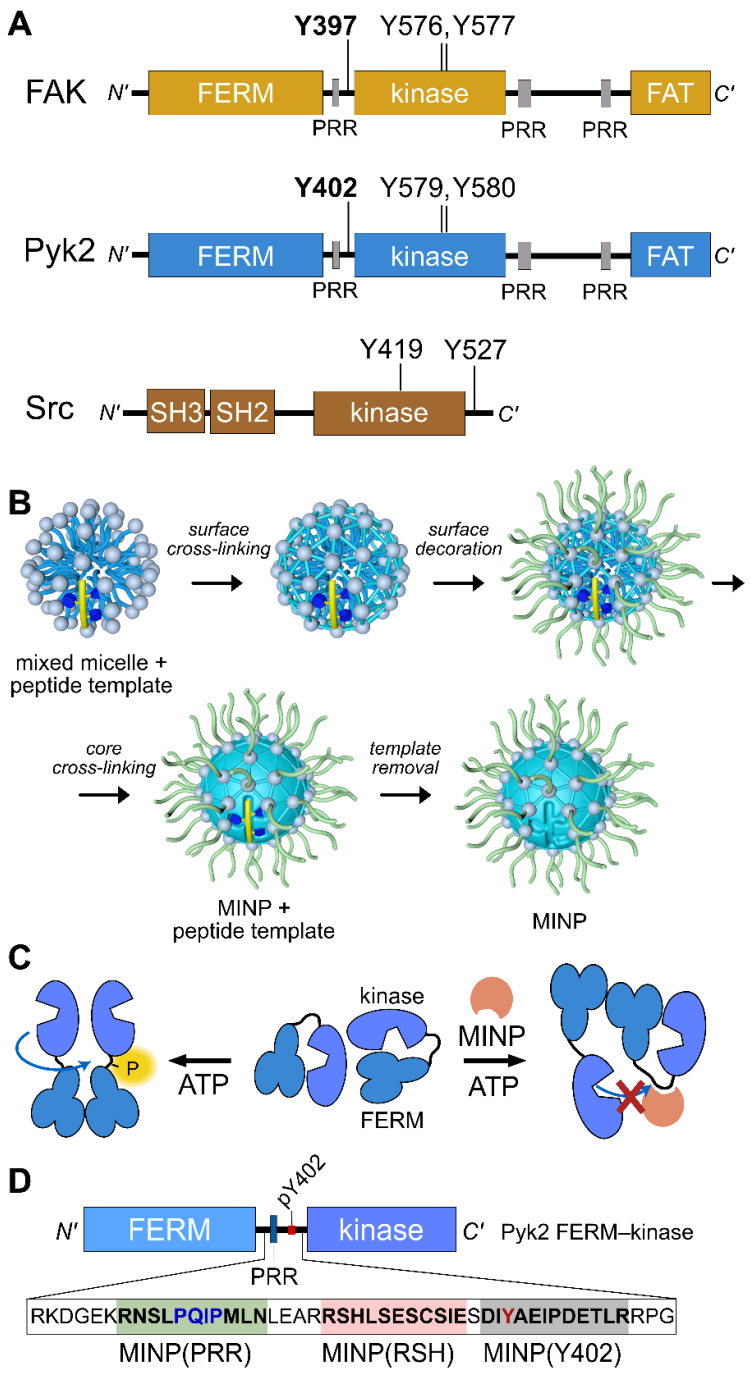

Figure 1. Tyrosine kinase regulatory features probed by MINPs (A) Domain organization of Pyk2, FAK, and Src kinase. Proline-rich regions (PRR) and phosphoacceptor tyrosines are annotated with linker autophosphorylation sites in bold. (B) Cartoon representation of peptide templated MINP preparation. Mixed micelles with functional monomers are cross-linked around peptide (yellow and blue) to afford a binding pocket with shape and functional group complementarity. Adapted from Li, *et al* (2021)[17]. (C) Schematic model for MINP-mediated inhibition of Pyk2 autophosphorylation. (D) Pyk2 FERM−kinase construct highlighting linker sequences used for MINP imprinting.

Notwithstanding activation differences, key regulatory mechanisms are shared between Pyk2 and FAK. Both kinases are autoinhibited by engagement of the FERM domain with the kinase C-lobe[18,19]. The FERM domain suppresses kinase activity by obscuring access to the kinase activation loop and blocking protein substrate docking. The autoinhibitory conformation is relieved by stimuli such as integrin engagement for FAK or calcium signaling for Pyk2. Stimulated conformational changes expose the kinase active site and trigger the autophosphorylation of a key tyrosine (FAK Y397, Pyk2 Y402) in the FERM–kinase linker[1,12]. The phospho-Y397 and a neighboring proline-rich repeat create a scaffold for signal effectors like Src kinase[20,21]. The engagement of the Src SH2 and SH3 domains with the FERM–kinase linker leads to Src-mediated phosphorylation of a pair of activation loop tyrosines. Phosphorylation of the activation loop ultimately enhances the catalytic activity, which in turn promotes the phosphorylation of downstream targets[22,23].

Although the mechanistic details of Pyk2 activation are obscured by limited high-resolution structural models, investigations dissecting Pyk2 regulation revealed key features[24–26]. Pyk2 exhibits intrinsic autophosphorylation independent of Src activity. Autophosphorylation is sufficient for Src to dock and outcompete the dynamic FERM-kinase autoinhibitory interface to phosphorylate the Pyk2 activation loop tyrosines (Y579, Y580). These observations underscore the intrinsic dynamics of the Pyk2 autoinhibitory conformation and highlight the importance of the accessibility of linker residue Y402 for the maturation of the Pyk2–Src activation complex.

Given the innate capacity of Pyk2 for autophosphorylation, the regulatory factors governing commitment to activation remain elusive. In FAK, the autophosphorylation site Y397 and surrounding residues are constrained in an antiparallel strand of a small FERM domain beta sheet[18]. Likewise, the neighboring proline-rich repeat makes intramolecular contacts with the FERM domain[27]. To date, it is unknown whether the autophosphorylation site of Pyk2 is also constrained via secondary structure. Additionally, the regulatory contributions of the Src SH2 and SH3 domains in the Pyk2 activation complex are unclear. To gain insight into the dynamics and signaling scaffolding of the Pyk2 autophosphorylation site, we employed chemical probes and biochemical characterizations, including peptide-binding molecularly imprinted nanoparticles (MINPs), mutagenesis, and activity profiling. MINPs are nanoparticle probes prepared from cross-linkable micelles containing template molecules and functional monomers

that interact with the templates through noncovalent or reversible covalent bonds (Figure 1B and Scheme S1). Template removal yields cavities (i.e., imprinted sites) with shapes and interaction networks complementary to the target molecule[28,29]. These “plastic antibodies” can bind peptides with high affinity (i.e., low nanomolar dissociation constants) and distinguish closely related amino acids such as leucine/isoleucine[28], aspartate/glutamate[30], and lysine/arginine[31]. The capacity for exquisite specificity enables MINPs to inhibit specific post-translational modifications[17,32] or probe the functional role of a specific peptide sequence[29]. Hence, we investigated the intricate mechanisms regulating Pyk2 activation by leveraging the distinctive features of MINPs to selectively target and probe specific Pyk2 regulatory features (Figure 1C).

Ultimately, our study provides new insights into Pyk2 regulation by revealing that the Y402 site is conformationally constrained in the autoinhibited state due to the formation of a short beta-sheet with the FERM domain. Disruption of this regulatory substructure results in trans autophosphorylation of the Y402 site, allowing Src docking and subsequent Src-mediated activation loop phosphorylation of Pyk2. Our findings clarify mechanisms of Pyk2 regulation and activation while demonstrating that MINPs can serve as effective conformational probes and chemical tools to investigate protein–protein interactions.

Results

The site of Pyk2 autophosphorylation is constrained via secondary structure

Previously, we reported on the efficacy of MINPs for controlling kinase activity by selective inhibition of kinase target phosphorylation sites (Figure 1C). Briefly, we found that MINPs targeting the Y402 site and neighboring regions could significantly inhibit Pyk2 autophosphorylation, albeit to varying degrees depending on the specific MINP binding targets. Intriguingly, our results showed that MINP(Y402), which was designed to target the Y402 site directly, exhibited weaker inhibitory potency than MINP(PRR) and MINP(RSH) (Figure 1D). We hypothesized that the reduced inhibitory activity of MINP(Y402) may reflect lower accessibility of the autophosphorylation site in the inhibited Pyk2 FERM−kinase basal conformation[17].

We sought to explore the correlation between MINP inhibitor potency and the accessibility of the Y402 site in the Pyk2 basal state. We first examined an AlphaFold-derived model of the autoinhibitory conformation of Pyk2[33,34] (Figure 2A). The AlphaFold-derived Pyk2 model reproduced the beta strands adhering the autophosphorylation site to the FERM domain in autoinhibited FAK by X-ray crystallography[18]. The model enabled us to identify residues potentially responsible for stabilizing the beta sheet and sequestering the autophosphorylation site. We assessed residue-specific contributions to the stabilization of the putative interaction between the FERM domain and the FERM−kinase linker by testing a disruptive variant E404P, predicted to enhance the autophosphorylation rate. Surprisingly, we found that E404P Pyk2 variant exhibits an autophosphorylation rate similar to WT Pyk2 FERM−kinase (Figure 2B and S1). We considered two possible explanations for this observation. Pyk2 regulation may differ from FAK, and Y402 sequestration does not limit basal autophosphorylation. Alternatively, the local structure constraining Y402 may be stabilized by multiple cooperative interactions, and the E404P substitution is insufficient to disrupt and liberate the linker. Importantly, kinase specificity for the local autophosphorylation motif remained a factor, and further residue substitutions risked perturbating recognition by the kinase active site.

To further interrogate the regulatory role of autophosphorylation site sequestration, we tested the inhibitory effects of site-specific MINPs. We assessed whether the E404P variant would present

a more accessible binding site for MINP(Y402) and thus enhance inhibitory potency (Figure 2C and S2). *In vitro* kinase assays of the WT and E404P Pyk2 FERM−kinase revealed that MINP(Y402) inhibited the autophosphorylation of the E404P Pyk2 variant far more effectively than WT Pyk2. Specifically, at a Pyk2:MINP ratio of 1:6, we observed near-complete inhibition of autophosphorylation of the E404P variant of Pyk2, while the wild-type (WT) Pyk2 phosphorylation was inhibited by only 30%. A non-imprinted nanoparticle (NINP) exhibited negligible inhibition. The enhanced inhibition potency of MINP(Y402) towards the E404P Pyk2 variant supports the hypothesis that the Y402 site and surrounding residues are constrained in a β-sheet conformation in the Pyk2 basal state. Thus, despite the sequence mismatch generated by the E404P Pyk2 mutation, the local structural perturbation in the Pyk2 FERM−kinase linker affords a better binding site for MINP(Y402). Based on the observed differential impact of MINP inhibition between the linker targets, we inferred that MINPs can differentiate between local polypeptide accessibility and/or conformations, emphasizing the ability of nanoparticle imprinting to recognize and bind to specific structural features beyond the primary amino acid sequence.

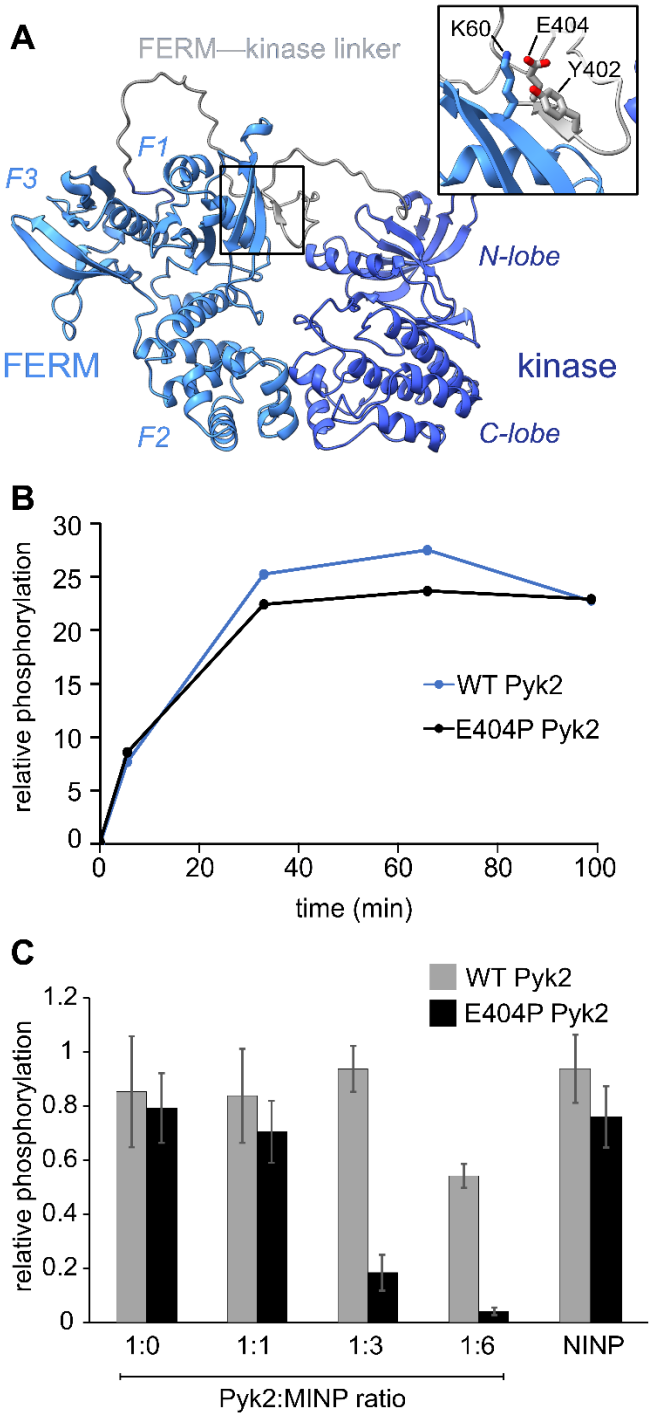

Figure 2. Pyk2 kinase regulatory conformations probed by molecularly imprinted nanoparticles. (A) AlphaFold-derived structural model of Pyk2 FERM−kinase with inset detailing the small β-sheet constraining Y402 in the Pyk2 linker segment colored in gray. (B) Kinase activity time course of WT and E404P Pyk2 FERM−kinase (0.5 μM). Tyrosine phosphorylation was detected via Western blotting with anti-phosphotyrosine primary antibody (PY20). (C) Inhibition of Pyk2 autophosphorylation by MINP(Y402) at protein:MINP ratios of 1:1, 1:3, and 1:6, with the NINP as the control at 1:6 ratio. Pyk2 concentration was fixed at 0.5 μM, and autophosphorylation was assessed 5 min after reaction initiation with ATP. Tyrosine phosphorylation was detected by dot immunoblotting with anti-phosphotyrosine primary antibody (PY20). Activity assay replicates (n = 3-5) represent independent reactions with error bars signifying standard deviation.

Conformational context modulates Pyk2 autophosphorylation via FERM domain

Our investigation into the regulation of Pyk2 autophosphorylation by MINPs revealed a reduced accessibility of the Y402 site within the inhibited conformation of Pyk2 FERM−kinase, presumably due to secondary structure engagement with the FERM domain. To further explore factors stabilizing Y402 sequestration, we returned to the AlphaFold-derived model of Pyk2 which draws on the reported autoinhibitory conformation of FAK (Figure 2A). The modeled Pyk2 FERM−kinase indicates an electrostatic sidechain interaction between FERM F1 subdomain residue K60 and linker residue E404. To test the contribution of Pyk2 K60 residue in stabilizing the secondary structure constraining Y402, we engineered alanine (K60A) and proline (K60P) variants of Pyk2 FERM−kinase construct. We investigated the impact of K60 variants on Pyk2 autoinhibition by monitoring autophosphorylation over a 30-minute time course (Figure 3A and S3). Our results revealed that the K60A variant exhibited a >5-fold increase in autophosphorylation compared to WT Pyk2. Strikingly, introducing a proline at the K60 position led to an even higher increase in Pyk2 autophosphorylation (>10-fold increase), implying complete disruption of the β-sheet conformation.

The canonical mechanism for full activation of autophosphorylated Pyk2 involves Src docking and subsequent activation loop phosphorylation at Pyk2 residues Y579 and Y580[25,26,35]. Given the pronounced increase in Pyk2 autophosphorylation upon disruption of the putative FERM:linker interface, we tested whether a K60 variant also impacted the phosphorylation status of the activation loop. We monitored site-specific phosphorylation in WT and K60P Pyk2 FERM−kinase. Blotting with site-specific antibodies revealed that the autophosphorylation target of the K60P variant was primarily the FERM−kinase linker residue Y402 (Figure 3B and S4). Similar to WT Pyk2, the K60P variant exhibited negligible autophosphorylation of its own activation loop.

Our results show that variants designed to disrupt FERM—kinase linker sequestration can increase MINP access or promote autophosphorylation. We surmised that the disruptive variants increase conformational accessibility of the linker autophosphorylation site. However, perturbing

remote FERM:linker contacts could also destabilize the autoinhibitory interface between FERM F2 and kinase C-lobe subdomains (Figure 2A)[18,19]. Indeed, previous studies established that disruption of the Pyk2 FERM F2:kinase C-lobe interface leads to increased autophosphorylation[26]. Hence, we sought to test whether the K60P mutation disrupts the global autoinhibitory conformation of Pyk2. We employed global hydrogen/deuterium exchange mass spectrometry (HDX-MS) to monitor the general uptake of deuterium throughout the intact protein. Our results revealed negligible differences in global exchange between WT and K60P Pyk2 FERM−kinase (Figure 3C). In contrast, targeted disruption of the FERM F2:kinase C-lobe autoinhibitory interface has been shown to increase global H/D exchange by 20 – 40 deuterons[19]. Taken together, we conclude that point mutations in the FERM domain (e.g., K60P Pyk2) disrupt main chain H-bonding and ion pairing, liberating the linker segment harboring autophosphorylation site Y402. Interestingly, when challenged to predict the architecture of the K60P variant of Pyk2, AlphaFold consistently generates models with a disengaged, conformationally flexible FERM—kinase linker (Figure 3D).

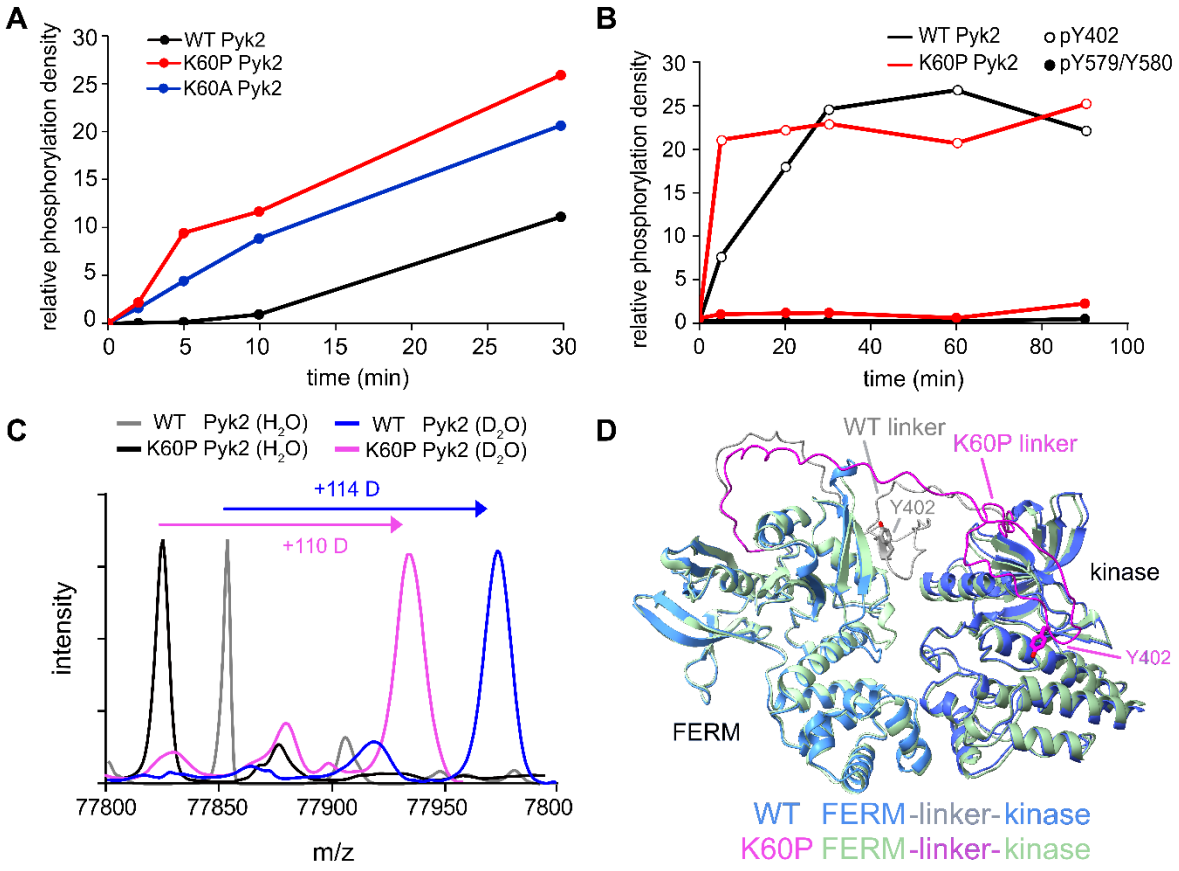

Figure 3. FERM domain variants modulate Pyk2 autophosphorylation (A) Kinase activity time courses of WT Pyk2 FERM−kinase (0.5 μM) and variants K60P and K60A. Tyrosine phosphorylation was detected via Western blotting with pan-specific anti-phosphotyrosine primary antibody (PY20). (B) Site-specific phosphorylation was monitored by blotting with anti-phospho-PYK2 (pY579/Y580) or anti-phospho-PTK2B (pY402). Phosphorylation levels were quantified by densitometry. (C) Global HDX-MS spectra of WT and K60P Pyk2 FERM–kinase. Spectra include unlabeled (H_2O) WT (grey) and K60P (black) superimposed with 2.5 min D_2O exposure of WT (blue) and K60P Pyk2 (magenta). (D) AlphaFold (ver. 2.3.1) generated models of WT (blue) and K60P (green) Pyk2 autoinhibitory conformation. The FERM−kinase linker is highlighted with the Y402 site for WT (grey) and K60P (magenta).

MINP binding competes with tandem Src motifs for Pyk2−Src complex formation

The Pyk2-Src interaction is essential for the regulation of immune cell migration and also plays a key role in modulating the structural plasticity of synapses in neuronal cells[36,37]. The binding between Pyk2 and Src is a complex and highly regulated process that involves multiple protein domains and phosphorylation. Due to the similarity with FAK, the docking of Src to Pyk2 is thought to be mediated by the binding of tandem Src SH3 and SH2 domains to Pyk2 proline-rich region (PRR) and phosphorylated Y402, respectively. The engagement of Src SH3 and SH2 domains with the Pyk2 FERM—kinase linker is thought to be a critical prerequisite to disengagement of the autoinhibitory conformation and phosphorylation of the Pyk2 activation

loop (Figure S5). Indeed, substituting tyrosine (Y) with phenylalanine (F) at position 402 drastically impairs phosphorylation levels of Y579 and Y580 residues in Y402F Pyk2 variant (Figure 4A and S6).

With an interest in targeted strategies to interfere with specific protein-protein signaling interactions[36], we investigated the potential of MINPs to selectively target specific Pyk2 docking sites and disrupt the formation of the Pyk2−Src activation complex. Specifically, we hypothesized that MINPs imprinted with either phospho-Y402 sequence or PRR sequence (Figure 4B) could outcompete the tandem Src motifs for Pyk2 binding. For this purpose, we assessed the inhibition of Src-mediated phosphorylation of Pyk2 activation loop tyrosines (Y579/Y580) in the presence of MINP(pY402) and MINP(PRR) alone or in combination. First, WT Pyk2 FERM–kinase was preincubated with ATP to allow for basal autophosphorylation to fully phosphorylate the Y402 site. Phospho-Y402 Pyk2 was pre-incubated with MINP or NINP followed by addition of Src. The impact of MINPs on Src-mediate Pyk2 activation loop phosphorylation was monitored over a time course using site-specific activation loop anti-phosphotyrosine (pY579/Y580) antibodies. Our results reveal that blocking either the Src SH3 or SH2 domain binding site in Pyk2 leads to substantial inhibition of Src-mediated phosphorylation of Pyk2 activation loop tyrosines (Figure 4D and S8). MINP(pY402) exhibited a more potent inhibition of Src activity than MINP(PRR). Interestingly, the combination of MINP(pY402) and MINP(PRR) resulted in comparable levels of inhibition to that achieved by MINP(pY402) alone. Thus, motif-specific MINP inhibition suggests that Src SH2 recognition of Pyk2 phosho-Y402 plays a critical role in nucleating the Src−Pyk2 activation complex. Nevertheless, the significant inhibition by MINP(PRR) reveals that blocking access to the Pyk2 PRR is sufficient for disruption of Src-mediated Pyk2 activation.

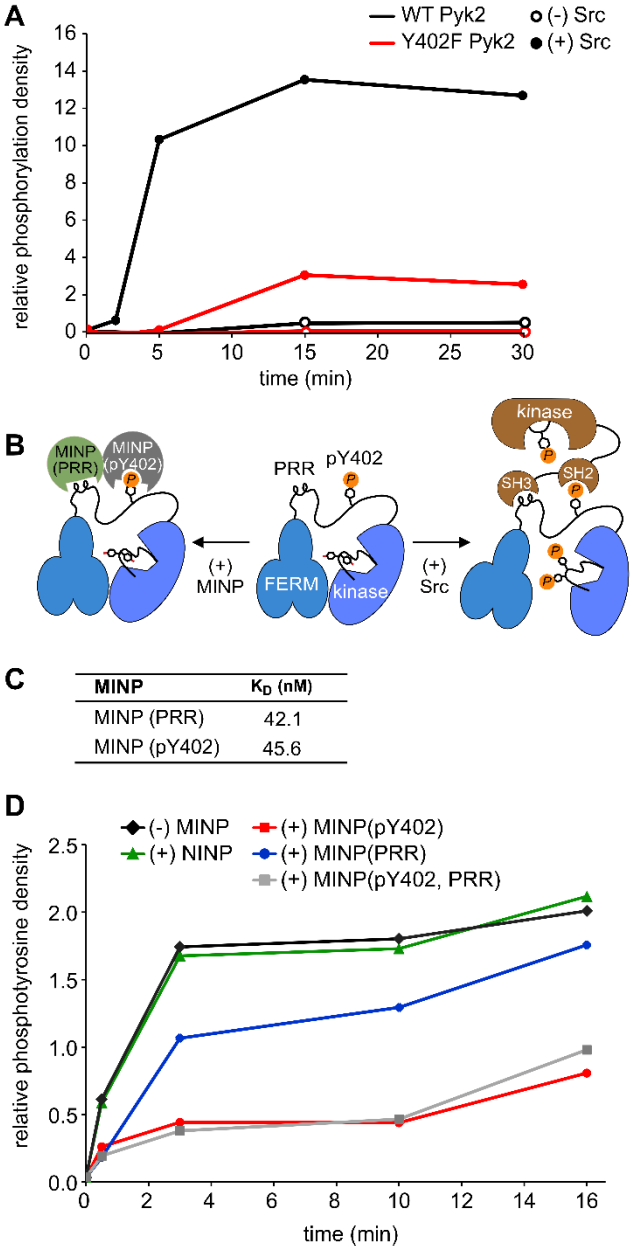

MINP	K_D (nM)
MINP (PRR)	42.1
MINP (pY402)	45.6

Figure 4. Interaction sites in the Pyk2−Src complex probed by MINPs. (A) Kinase activity time course of WT or Y402F Pyk2 FERM−kinase (0.5 μM) in the presence or absence of Src (0.5 μM). Site-specific phosphorylation was detected by blotting with anti-phospho-PYK2 (pY579/Y580). (B) Schematic illustrating MINP-mediated inhibition of Pyk2 activation loop phosphorylation. (C) Dissociation constants measured via isothermal titration calorimetry for MINP(pY402) and MINP(PRR) with the corresponding peptide template. (D) Activation loop phosphorylation (Y579/Y580) of phospho-Y402 Pyk2 FERM−kinase (1 μM) preincubated with MINP. Src (0.5 μM) was added 3 min after MINP equilibration. At various time points, samples were quenched and blotted with anti-phospho-Y579/Y580 primary antibody and quantified by densitometry.

Discussion

Pyk2 activation is regulated by a complex interplay of factors, including autoinhibitory interdomain interactions, multiple phosphorylation events, and Src recruitment. However, the molecular details and coordination of these mechanisms that regulate Pyk2 activity remain incomplete. In this study, we gain insights into the regulatory features governing Pyk2 Y402 autophosphorylation and the role of phosphoY402 and proline-rich regions in modulating Src interaction. By integrating molecularly imprinted nanoparticles (MINPs) and targeted mutagenesis with structural models of Pyk2, we also highlighted the potential of MINPs as effective conformational probes and chemical tools to investigate signaling protein regulatory processes.

Previously, in an effort to characterize MINPs designed to control Pyk2 autophosphorylation, we noticed decreased accessibility of MINPs targeting the Y402 linker site in the Pyk2 FERM−kinase autoinhibited conformation[17]. We reasoned that the Pyk2 autophosphorylation site in the inactive conformation may be engaged in a β-sheet, similarly to the paralogous FAK Y397 residue[18]. In this study, we tested this idea with newly designed MINPs and Pyk2 variants designed to disengage the putative secondary structure around Y402. We found that a proline substitution in the Pyk2 FERM−kinase linker strikingly enhanced the efficacy of MINP-mediated inhibition of Pyk2 autophosphorylation, likely due to the release of the Y402 regional β-strand (Figure 2). Notably, the β-strand conformation is uniquely resistant to MINP recognition due to its fully extended torsion angles that differ significantly from the free, flexible peptide template imprinted on the MINP. This observation suggests that the MINP templating strategy can be leveraged to differentiate local polypeptide conformations and selectively target specific conformational states of proteins such as kinases.

Given the MINP-based profiling that revealed autophosphorylation site sequestration, we dissected the interactions stabilizing the low accessibility conformation of Y402 in a Pyk2 autoinhibitory state. The autophosphorylation sites in both FAK and Pyk2 are located within a conserved YAEI sequence closely matching the Src SH2 consensus binding motif (pYEEI)[38] (Figure 1B). In the crystallography-derived FAK FERM–kinase structural model[18], the E399 sidechain (E404 in Pyk2) is within range (~3 Å) for electrostatic interaction with the FERM

domain R57 sidechain (K60 in Pyk2). Although the impact of this apparent salt bridge in FAK remains unknown, substituting K60 in Pyk2 to a non-polar residue significantly increases the Pyk2 autophosphorylation rate. We therefore conclude that interdomain sidechain ion pairing stabilizes the restrictive secondary structure and downregulates the intrinsic Pyk2 autophosphorylation activity. Indeed, HDX-MS confirmed that the impact of the K60P variant is focused on Y402 accessibility. WT and K60P Pyk2 FERM−kinase constructs exhibited no significant differences in global dynamics (Figure 3C). While current versions of AlphaFold harbor limitations in predicting the structural impact of missense mutations[39], we were intrigued to see that the top AlphaFold models generated for the K60P Pyk2 FERM−kinase variant all feature liberated FERM—kinase linkers, unconstrained by FERM domain interactions (Figure 3D). Together, MINP profiling, site-directed mutagenesis studies, and global HDX-MS indicate that release of the Y402 site from a restrictive FERM domain interaction strongly promotes autophosphorylation without destabilizing the primary FERM:kinase autoinhibitory interface.

The Pyk2−Src activation complex is known to be the arbiter of downstream Pyk2 signaling cascades. Indeed, autophosphorylated Pyk2 exhibits tandem phosphotyrosine and proline-rich motifs in the FERM—kinase linker ideally spaced for cooperative Src SH2/SH3 interactions. Presentation of high affinity Src SH2 and SH3 binding motifs can promote Src activation by relieving inhibitory intramolecular Src SH2/SH3 interactions[40]. The importance of the Src docking interactions for Pyk2 activation complex maturation prompted us to investigate the potential of MINPs to inhibit each individual docking site. Our results demonstrate that MINPs targeting either Src-binding motifs in Pyk2 can successfully outcompete Src domains and inhibit Src-mediated Pyk2 activation loop phosphorylation. We also observed an intriguing contrast between the activities of MINP(Y402), targeting the Pyk2 autophosphorylation site, and MINP(pY402), targeting Src SH2 docking via the same site modified by phosphorylation. MINP(Y402) inhibition is muted by the apparent inaccessibility of the unphosphorylated Y402 region, presumably via integration into a β-sheet with the FERM domain (Figure 2C). MINP(pY402), however, readily recognized the phosphotyrosine linker motif and potently inhibited Src activity. Targeted mutagenesis highlighted the role of ion pairing in stabilizing the sequestration of the Y402 region (Figure 3). We speculate that Y402 phosphorylation dissociates the linker region from the FERM β-sheet due to local conformational changes associated with the

addition of additional negative charge. The increased accessibility of the linker upon Y402 phosphorylation may be important for Src SH2 engagement.

Notably, despite similarly high affinities (Figure 4C and S7), MINP(pY402) and MINP(PRR), inhibit Src phosphorylation to different degrees (Figure 4D). The higher potency of MINP(pY402) indicates that Src SH2 docking is critical for nucleating the Pyk2−Src complex formation, while the Pyk2 PRR contributes additional stability via Src SH3 binding. Consistent with our results, Thomas et al.[20], investigating the binding requirements of Src for FAK, found that the FAK Y397F variant did not co-immunoprecipitate with Src, while an alanine variant targeting the FAK PRR did co-immunoprecipitate with Src, albeit to a lesser extent than the WT FAK. Together, these findings indicate the critical role of the Src SH3-binding site of Pyk2 in the efficient formation of the Src−Pyk2 complex and highlight the potential of MINP as a tool to probe binding sites in protein complexes.

Ultimately, we demonstrate that MINPs can be used to selectively target specific conformations in the Pyk2 autoinhibited state, providing insights into the regulation of Pyk2 activation. The identification of a proline mutation in the Pyk2 FERM−kinase linker that enhances the efficacy of MINP-mediated inhibition of Pyk2 autophosphorylation indicates that the Y402 region is constrained in a β-sheet conformation in the Pyk2 basal state. MINPs targeting each Src binding motif also successfully displaced Src SH2 and SH3 domains. Taken together, the selective blockage of unique Pyk2 regulatory features by tailored MINPs highlights the potential for deploying MINPs as surgical inhibitors of specific signaling subsystems. Indeed, both FAK and Pyk2 are archetypal signaling hubs that serve multiple roles as signaling enzymes and organizational scaffolds of multiprotein signaling complexes[35]. We envision that designer MINPs could be valuable probes for dissecting specific signaling functions in higher-order signaling complexes.

Methods

Preparation and Imprinting of Functionalized MINPs

Preparation of the functionalized MINPs was carried out as previously reported[17]. For nomenclature clarity, MINP11a and MINP11c from Ref. 17 were renamed MINP(PRR) and MINP(Y402), respectively, in this study. MINP(pY402) was synthesized for this study using a phosphorylated peptide (DIpYAEIPDETLR) mimicking the linker sequence surrounding the Pyk2 autophosphorylation site Y402. The MINP(pY402) template peptide was phosphorylated by a 3 h, 37 °C incubation of peptide with 1 μM Pyk2 FERM−kinase in buffer consisting of 50 mM HEPES pH 7.4, 150 mM NaCl, 8 mM $MgCl_2$, 5% glycerol, and 4 mM ATP. Peptide phosphorylation was confirmed via liquid chromatography-mass spectrometry (LC-MS).

MINPs were prepared with functional monomers using the following stoichiometries in the formulation: 1.5:1 for **1**/carboxylate or phosphate on the peptide template, 1:1 for **2**/arginine, and 1:1 for **3**/amine (Scheme S1). Compound **1** in methanol (37.5 μL of a 5.5 mg/mL solution, 0.6 μmol), **2** in methanol (50 μL of a 9.5 mg/mL solution, 0.8 μmol), **3** in methanol (25 μL of a 6.7 mg/ mL solution, 0.4 μmol), and peptide in methanol (0.4 μmol) were added to a glass vial and diluted with methanol to a final volume of 500 μL. The mixture was vortexed for 30 min before the solvent was removed under vacuum. A micellar solution of surfactant **4** (9.3 mg, 20 μmol) in H_2O (2.0 mL) was added to the above template–FM complex, followed by the addition of divinylbenzene (2.8 μL, 20 μmol) and photoinitiator 2,2-dimethoxy-2-phenylacetophenone in DMSO (10 μL of a 12.8 mg/mL solution, 0.5 μmol). The mixture was subjected to ultrasonication for 10 min before compound **5** (4.1 mg, 24 μmol), $CuCl_2$ in H_2O (10 μL of 6.7 mg/mL solution, 0.5 μmol) and sodium ascorbate in H_2O (10 μL of 99 mg/mL solution, 5 μmol) were added. The reaction mixture was stirred slowly at room temperature for 12 h. After incubation, compound **6** (10.6 mg, 40 μmol), $CuCl_2$ in H_2O (10 μL of 6.7 mg/mL solution, 0.5 μmol), and sodium ascorbate in H_2O (10 μL of 99 mg/mL solution, 5 μmol) were added. The mixture was stirred at room temperature for another 6 h, then purged with nitrogen for 15 min. The vial was sealed with a rubber stopper, degassed and refilled with nitrogen three times, and irradiated in a Rayonet reactor for 12 h. Finally, the reaction mixture was poured into acetone (8 mL). The precipitate was collected by centrifugation and washed with a mixture of acetone/water

(5 mL/1 mL) three times, methanol/acetic acid (5 mL/0.1 mL) three times, acetone (5 mL) twice, and then dried in air to afford the final MINPs. Typical yields were > 80%.

ITC Titration Experiments

A solution of the titrating peptide was injected in equal steps of 10 μL into the sample cell containing the MINP solution. In the ITC curves presented, the top panel shows the raw calorimetric data. The area under each peak represents the amount of heat generated at each injection and is plotted against the molar ratio of the peptide to the MINP (Figure S7). The solid line is the best fit of the experimental data to the sequential binding of *N* binding sites on the MINP. The heat of dilution, obtained by adding the titrating solution to the buffer, was subtracted from the heat released during the binding. Binding parameters were generated from curve fitting using Microcal Origin 7.0.

Protein Purification

Protein constructs used in this study have been previously outlined[26]. K60P, K60A, E404P, and Y402F Pyk2 FERM−kinase mutants were generated using the QuikChange (Agilent Genomics) site-directed mutagenesis strategy. All variants were confirmed by DNA sequencing. Purification of all proteins used in this study was performed as previously described[26]. Briefly, Pyk2 FERM−kinase constructs (WT, K60P, K60A, E404P, and Y402F) or His_6-SUMO-Src (residues 1-536) were co-transformed with the YopH phosphatase plasmid (pESU009), encoding tyrosine phosphatase domain (residues 177 – 463), into *E. coli* NiCo21(DE3) cells to generate homogenous, dephosphorylated Pyk2 or Src proteins. After overnight expression at 18°C, cells were harvested and lysed by sonication in lysis buffer composed of 50 mM Tris pH 8, 25 mM NaCl, 20 mM imidazole, 1 mM PMSF, 5 mM EDTA, 5% glycerol, 2.5 mM β-mercaptoethanol, and protease inhibitors. Lysates were cleared by ultracentrifugation at 80,000 ×g for 15 min at 4 °C. His_6-tagged Pyk2 or His_6-tagged Src was isolated by Ni-NTA affinity chromatography, followed by cleavage of the His_6-SUMO tag using His_6-tagged Ulp1 protease. A subtractive passage through Ni-NTA resin removed the protease and cleaved His_6-SUMO tag. The purified Pyk2 or Src constructs were concentrated via centrifugal filtration and further purified by gel filtration chromatography in SEC buffer composed of 50 mM HEPES pH 7.4, 150 mM NaCl,

5% glycerol, 5 mM TCEP. Purified Pyk2 constructs or Src was concentrated, aliquoted, frozen in liquid nitrogen, and stored at -80 °C.

Kinase Assays

Kinase reactions were performed using a final concentration of 0.5 μM or 1 μM for wild type (WT) or Pyk2 FERM–kinase variants in a buffer consisting of 50 mM HEPES pH 7.4, 150 mM NaCl, 8 mM $MgCl_2$, 5% glycerol. The secondary structure in Pyk2 was investigated in the presence of MINP(Y402) or non-imprinted nanoparticle (NINP). MINP(Y402) was added to individual kinase reactions at a range of final concentrations (1, 3, or 6 μM), whereas NINP was added at 6 μM. Stock solutions were sonicated before use for 5min. Kinase/MINP mixtures were pre-equilibrated at 20 °C for 5 min. Kinase activity was initiated by adding 4 mM ATP (final concentration) and quenched at specific time points with 10 mM EDTA followed by heat denaturation at 90°C for 60 seconds.

To investigate the Pyk2–Src interaction, we performed kinase assays similar to the above protocol. Specifically, WT Pyk2 FERM−kinase (0.5 μM) was pre-incubated with kinase buffer containing 4 mM ATP for 20 minutes at 20 °C to ensure complete autophosphorylation at Y402 residue in Pyk2. MINPs (pY402) and (PRR) were subsequently added to the reaction mixture at a final concentration of 6 μM and incubated for 3 minutes. Src was then added to the reaction to monitor the phosphorylation of Y579/Y580 in Pyk2. Samples were quenched at various time points with 10 mM EDTA (final concentration).

General phosphotyrosine production was assessed via Western or Dot blotting using primary mouse anti-phosphotyrosine antibody (PY20) followed by goat-anti-mouse HRP conjugated secondary antibody. Site-specific phosphotyrosine blotting was performed with anti-phospho-PTK2B (pY402) or anti-phospho-PYK2 (pY579/pY580) primary antibodies with the goat anti-mouse HRP-conjugated secondary antibody. Blots were imaged with a chemiluminescent substrate (Pierce). Phosphotyrosine density was quantified by densitometry (Image Lab, Bio-Rad).

Global Hydrogen/Deuterium Exchange-Mass Spectrometry (HDX-MS)

Global HDX-MS was initiated by diluting Pyk2 FERM-kinase variants (80 pmol) into D_2O buffer composed of a final concentration of 150 mM KCl, 50 mM HEPES, 5 mM DTT (pD 7.4), and 89% D_2O. Exchange reaction mixtures were incubated at 21 °C. At time point 2.5 min, labeling reactions were quenched to pH 2.5 by addition of 0.25M sodium phosphate (final concentration). Non-exchanged samples were acquired in matched H_2O buffers to establish intact mass baselines for each variant. Quenched samples were immediately injected (2 µL) into an ACQUITY UPLC H-class instrument coupled in line to an ESI-Q-TOF Synapt G2-Si instrument (Waters). Mobile phases consisted of solvents A (HPLC-grade aqueous 0.1% formic acid) and B (HPLC-grade acetonitrile and 0.1% formic acid). Exchange samples were desalted on a C4 column (5 µm, 1 mm × 50 mm; Restek) with 30% solvent B for 1 min at a flow rate of 400 µL/min. Intact protein was eluted with a rapid gradient ramp from 35% to 75% solvent B over 3 min. MS data were collected in positive ion, MS continuum, and resolution mode with an *m*/*z* range of 300–4000. The intact mass of each exchange time point was deconvoluted from multiple charge states using the MaxEnt1 function of MassLynx (Waters).

Quantification and statistical analysis

The information regarding quantification and statistical analysis is indicated in the figure legends. For kinase assays, n = 3-5 where n is the number of replicate assays/measurements. The individual values were plotted with the mean and standard deviation on GraphPad Prism 9.

Acknowledgements

We thank Joel Nott of the Iowa State University Protein Facility for mass spectrometry support. This research was funded by the National Science Foundation, Division of Molecular and Cellular Biosciences grant 1715411 and Division of Materials Research grants 2308625 and 2002659.

References

1. Lev, S., Moreno, H., Martinez, R., Canoll, P., Peles, E., Musacchio, J.M., Plowman, G.D., Rudy, B., and Schlessinger, J. (1995). Protein tyrosine kinase PYK2 involved in Ca^{2+}-induced regulation of ion channel and MAP kinase functions. Nature *376*, 737–745. 10.1038/376737a0.

2. Avraham, S., London, R., Fu, Y., Ota, S., Hiregowdara, D., Li, J., Jiang, S., Pasztor, L.M., White, R.A., Groopman, J.E., et al. (1995). Identification and Characterization of a Novel Related Adhesion Focal Tyrosine Kinase (RAFTK) from Megakaryocytes and Brain. J. Biol. Chem. *270*, 27742–27751. 10.1074/jbc.270.46.27742.

3. Sasaki, H., Nagura, K., Ishino, M., Tobioka, H., Kotani, K., and Sasaki, T. (1995). Cloning and Characterization of Cell Adhesion Kinase β, a Novel Protein-tyrosine Kinase of the Focal Adhesion Kinase Subfamily. J. Biol. Chem. *270*, 21206–21219. 10.1074/jbc.270.36.21206.

4. de Pins, B., Mendes, T., Giralt, A., and Girault, J.A. (2021). The Non-receptor Tyrosine Kinase Pyk2 in Brain Function and Neurological and Psychiatric Diseases. Front. Synaptic Neurosci. *13*, 1–27. 10.3389/fnsyn.2021.749001.

5. Sun, C.K., Man, K., Ng, K.T., Ho, J.W., Lim, Z.X., Cheng, Q., Lo, C.-M., Poon, R.T., and Fan, S.-T. (2008). Proline-rich tyrosine kinase 2 (Pyk2) promotes proliferation and invasiveness of hepatocellular carcinoma cells through c-Src/ERK activation. Carcinogenesis *29*, 2096–2105. 10.1093/carcin/bgn203.

6. Sbrana, F.V., Fiordi, B., Bordini, J., Belloni, D., Barbaglio, F., Russo, L., Scarfò, L., Ghia, P., and Scielzo, C. (2023). PYK2 is overexpressed in chronic lymphocytic leukaemia: A potential new therapeutic target. J. Cell. Mol. Med. *27*, 576–586. 10.1111/jcmm.17688.

7. Roelle, S., Grosse, R., Buech, T., Chubanov, V., and Gudermann, T. (2008). Essential role of Pyk2 and Src kinase activation in neuropeptide-induced proliferation of small cell lung cancer cells. Oncogene *27*, 1737–1748. 10.1038/sj.onc.1210819.

8. Lane, D., Matte, I., Laplante, C., Garde-Granger, P., Carignan, A., Bessette, P., Rancourt, C., and Piché, A. (2016). CCL18 from ascites promotes ovarian cancer cell migration through proline-rich tyrosine kinase 2 signaling. Mol. Cancer *15*, 58. 10.1186/s12943-016-0542-2.

9. Lang, D., Glukhov, A. V., Efimova, T., and Efimov, I.R. (2011). Role of Pyk2 in cardiac arrhythmogenesis. Am. J. Physiol. Circ. Physiol. *301*, H975–H983. 10.1152/ajpheart.00241.2011.

10. Zhu, J., Chu, S. feng, Peng, Y., Liu, D. dan, Chen, C., Jian, W. xuan, Sun, H. shuo, Feng, Z. ping, Zhang, Z., and Chen, N. hong (2021). Pyk2 inhibition attenuates hypoxic-ischemic brain injury in neonatal mice. Acta Pharmacol. Sin. 10.1038/s41401-021-00694-5.

11. Montalban, E., Al-Massadi, O., Sancho-Balsells, A., Brito, V., de Pins, B., Alberch, J., Ginés, S., Girault, J.A., and Giralt, A. (2019). Pyk2 in the amygdala modulates chronic

stress sequelae via PSD-95-related micro-structural changes. Transl. Psychiatry *9*. 10.1038/s41398-018-0352-y.

12. Goñi, G.M., Epifano, C., Boskovic, J., Camacho-Artacho, M., Zhou, J., Bronowska, A., Martín, M.T., Eck, M.J., Kremer, L., Gräter, F., et al. (2014). Phosphatidylinositol 4,5-bisphosphate triggers activation of focal adhesion kinase by inducing clustering and conformational changes. Proc. Natl. Acad. Sci. U. S. A. *111*. 10.1073/pnas.1317022111.

13. Bartos, J.A., Ulrich, J.D., Li, H., Beazely, M.A., Chen, Y., MacDonald, J.F., and Hell, J.W. (2010). Postsynaptic clustering and activation of Pyk2 by PSD-95. J. Neurosci. *30*, 449–463. 10.1523/JNEUROSCI.4992-08.2010.

14. Schaller, M.D. (2008). Calcium-dependent Pyk2 activation: a role for calmodulin? Biochem. J. *410*, 10–11. 10.1042/BJ20080133.

15. Man, K.N.M., Bartels, P., Henderson, P.B., Kim, K., Shi, M., Zhang, M., Ho, S.-Y., Nieves-Cintron, M., Navedo, M.F., Horne, M.C., et al. (2023). α1-Adrenergic receptor–PKC–Pyk2–Src signaling boosts L-type Ca2+ channel CaV1.2 activity and long-term potentiation in rodents. eLife *12*. 10.7554/eLife.79648.

16. Momin, A.A., Mendes, T., Barthe, P., Faure, C., Hong, S.B., Yu, P., Kadaré, G., Jaremko, M., Girault, J.A., Jaremko, Ł., et al. (2022). PYK2 senses calcium through a disordered dimerization and calmodulin-binding element. Commun. Biol. *5*, 1–15. 10.1038/s42003-022-03760-8.

17. Li, X., Palhano Zanela, T.M., Underbakke, E.S., and Zhao, Y. (2021). Controlling Kinase Activities by Selective Inhibition of Peptide Substrates. J. Am. Chem. Soc. *143*, 639–643. 10.1021/jacs.0c11566.

18. Lietha, D., Cai, X., Ceccarelli, D.F.J., Li, Y., Schaller, M.D., and Eck, M.J. (2007). Structural Basis for the Autoinhibition of Focal Adhesion Kinase. Cell *129*, 1177–1187. 10.1016/j.cell.2007.05.041.

19. Loving, H.S., and Underbakke, E.S. (2019). Conformational Dynamics of FERM-Mediated Autoinhibition in Pyk2 Tyrosine Kinase. Biochemistry *58*, 3767–3776. 10.1021/acs.biochem.9b00541.

20. Thomas, J.W., Ellis, B., Boerner, R.J., Knight, W.B., White, G.C., and Schaller, M.D. (1998). SH2- and SH3-mediated interactions between focal adhesion kinase and Src. J. Biol. Chem. *273*, 577–583. 10.1074/jbc.273.1.577.

21. Schaller, M.D., Hildebrand, J.D., Shannon, J.D., Fox, J.W., Vines, R.R., and Parsons, J.T. (1994). Autophosphorylation of the focal adhesion kinase, pp125FAK, directs SH2-dependent binding of pp60src. Mol. Cell. Biol. *14*, 1680–1688. 10.1128/mcb.14.3.1680-1688.1994.

22. Tachibana, K., Urano, T., Fujita, H., Ohashi, Y., Kamiguchi, K., Iwata, S., Hirai, H., and Morimoto, C. (1997). Tyrosine Phosphorylation of Crk-associated Substrates by Focal Adhesion Kinase. J. Biol. Chem. *272*, 29083–29090. 10.1074/jbc.272.46.29083.

23. Schaller, M.D., and Parsons, J.T. (1995). pp125FAK-dependent tyrosine phosphorylation of paxillin creates a high-affinity binding site for Crk. Mol. Cell. Biol. *15*, 2635–2645.

10.1128/MCB.15.5.2635.

24. Park, S.Y., Avraham, H.K., and Avraham, S. (2004). RAFTK/Pyk2 activation is mediated by trans-acting autophosphorylation in a Src-independent manner. J. Biol. Chem. *279*, 33315–33322. 10.1074/jbc.M313527200.

25. Zhao, M., Finlay, D., Zharkikh, I., and Vuori, K. (2016). Novel Role of Src in Priming Pyk2 Phosphorylation. PLoS One *11*, e0149231. 10.1371/journal.pone.0149231.

26. Palhano Zanela, T.M., Woudenberg, A., Romero Bello, K.G., and Underbakke, E.S. (2023). Activation loop phosphorylation tunes conformational dynamics underlying Pyk2 tyrosine kinase activation. Structure *31*, 447–475.E5. 10.1016/j.str.2023.02.003.

27. Marlowe, T., Dementiev, A., Figel, S., Rivera, A., Flavin, M., and Cance, W. (2019). High resolution crystal structure of the FAK FERM domain reveals new insights on the Druggability of tyrosine 397 and the Src SH3 binding site. BMC Mol. Cell Biol. *20*, 1–9. 10.1186/s12860-019-0193-4.

28. Awino, J.K., Gunasekara, R.W., and Zhao, Y. (2017). Sequence-Selective Binding of Oligopeptides in Water through Hydrophobic Coding. J. Am. Chem. Soc. *139*, 2188–2191. 10.1021/jacs.6b12949.

29. Zangiabadi, M., Ghosh, A., and Zhao, Y. (2023). Nanoparticle Scanners for the Identification of Key Sequences Involved in the Assembly and Disassembly of β-Amyloid Peptides. ACS Nano *17*, 4764–4774. 10.1021/acsnano.2c11186.

30. Fa, S., and Zhao, Y. (2018). Water-Soluble Nanoparticle Receptors Supramolecularly Coded for Acidic Peptides. Chem. - A Eur. J. *24*, 150–158. 10.1002/chem.201703760.

31. Fa, S., and Zhao, Y. (2019). General Method for Peptide Recognition in Water through Bioinspired Complementarity. Chem. Mater. *31*, 4889–4896. 10.1021/acs.chemmater.9b01613.

32. Li, X., Chen, K., and Zhao, Y. (2021). Sequence-Selective Protection of Peptides from Proteolysis. Angew. Chemie Int. Ed. *60*, 11092–11097. 10.1002/anie.202102148.

33. Jumper, J., Evans, R., Pritzel, A., Green, T., Figurnov, M., Ronneberger, O., Tunyasuvunakool, K., Bates, R., Žídek, A., Potapenko, A., et al. (2021). Highly accurate protein structure prediction with AlphaFold. Nature *596*, 583–589. 10.1038/s41586-021-03819-2.

34. Varadi, M., Anyango, S., Deshpande, M., Nair, S., Natassia, C., Yordanova, G., Yuan, D., Stroe, O., Wood, G., Laydon, A., et al. (2022). AlphaFold Protein Structure Database: massively expanding the structural coverage of protein-sequence space with high-accuracy models. Nucleic Acids Res. *50*, D439–D444. 10.1093/nar/gkab1061.

35. Walkiewicz, K.W., Girault, J.A., and Arold, S.T. (2015). How to awaken your nanomachines: Site-specific activation of focal adhesion kinases through ligand interactions. Prog. Biophys. Mol. Biol. *119*, 60–71. 10.1016/j.pbiomolbio.2015.06.001.

36. Zhu, X., Bao, Y., Guo, Y., and Yang, W. (2018). Proline-rich protein tyrosine Kinase 2 in inflammation and cancer. Cancers (Basel). *10*. 10.3390/cancers10050139.

37. Huang, Y.Q., Lu, W.Y., Ali, D.W., Pelkey, K.A., Pitcher, G.M., Lu, Y.M., Aoto, H., Roder, J.C., Sasaki, T., Salter, M.W., et al. (2001). CAKβ/Pyk2 kinase is a signaling link for induction of long-term potentiation in CA1 hippocampus. Neuron *29*, 485–496. 10.1016/S0896-6273(01)00220-3.

38. Zhou, S. (1993). SH2 domains recognize specific phosphopeptide sequences. Cell *72*, 767–778. 10.1016/0092-8674(93)90404-E.

39. Pak, M.A., Markhieva, K.A., Novikova, M.S., Petrov, D.S., Vorobyev, I.S., Maksimova, E.S., Kondrashov, F.A., and Ivankov, D.N. (2023). Using AlphaFold to predict the impact of single mutations on protein stability and function. PLOS One *18*, e0282689. 10.1371/journal.pone.0282689.

40. Roskoski, R. (2015). Src protein-tyrosine kinase structure, mechanism, and small molecule inhibitors. Pharmacol. Res. *94*, 9–25. 10.1016/j.phrs.2015.01.003.